# Developing convective heat transfer in helical pipes with finite pitch

**Shijie Liu and Jacob H. Masliyah**
Department of Chemical Engineering, University of Alberta, Edmonton, Canada

Simultaneous development of laminar Newtonian flow and heat transfer in helical pipes is numerically studied. The governing equations are fully parabolized in the axial direction and are written in an orthogonal helical coordinate system. For the special case of a torus, the numerical results for Nusselt number agree well with published data. The Nusselt number in the developing region is found to be oscillatory. The asymptotic Nusselt number and the thermal entrance length are correlated with the fluid Prandtl number and the flow Dean number, $Dn = Re\ \lambda^{1/2}$. Here Re is the flow Reynolds number and $\lambda$ is the dimensionless curvature ratio.

When torsion is dominant, the asymptotic Nusselt number decreases while the thermal developing length increases with $\gamma$, where $\gamma\ (=\eta\lambda^{-1/2}Dn^{-1/2})$ is the flow-pattern transition parameter for high Dean number flows. Here $\eta$ is the dimensionless torsion. When $\gamma$ is large, the asymptotic Nusselt number tends to the limits corresponding to a Poiseuille flow.

**Keywords:** curved pipe flow; secondary flow; convective heat transfer; laminar flow; Nusselt number; Dean number; developing flow

## 1. Introduction

Fluid flow and heat transfer in helically coiled pipes of constant circular cross section are important in many industrial processes. In terms of space conservation, helically coiled pipes can offer improved heat transfer efficiency in comparison to straight pipes. Owing to the complexity of the flow in helical pipes that have a finite pitch, most numerical and experimental studies deal with the special case of a torus, i.e., a helical pipe of zero pitch. These studies are summarized by Berger et al. (1983), Nandakumar and Masliyah (1986), Ito (1987), and Berger (1991).

For the case of a torus, simultaneous development of fluid flow and heat transfer was treated by Patankar et al. (1974). Developing heat transfer from a fully developed flow in a torus was studied by Tarbell and Samuels (1973) for the uniform wall temperature condition. Akiyama and Cheng (1974a, b) studied developing laminar forced convection for both uniform constant wall temperature and constant heat-flux conditions. They confirmed, in principle, the experimentally observed oscillations in the Nusselt number reported by Dravid et al. (1971), Balejova et al. (1977), and Janssen and Hoogendoorn (1978). The latter correlated the thermal entrance length and found it to be shorter than that for a straight pipe.

Fully developed flows in helical pipes of finite pitch were numerically studied by Liu (1992) and Liu and Masliyah (1993b). By employing a loose coiling analysis, these authors arrived at two controlling parameters, namely, the Dean number, Dn, and the Germano number, Gn. The Dean number is a measure of the ratio of the square root of the product of inertial and centrifugal forces to the viscous forces. The Dean number is given by $Dn = Re\ \lambda^{1/2}$. The Germano number, $Gn = Re\ \eta$, is a measure of the ratio of the twisting to the viscous forces.

Address correspondence to Professor Masliyah at the Department of Chemical Engineering, University of Alberta, Edmonton, Canada T6G 2G6.

Received 10 February 1993; accepted 2 September 1993



The Germano number is embedded in the body-centered peripheral velocity, $\xi = u_3 - Gn\, ru_1/h_1$, when $\lambda \to 0$. Although $\xi$ is not an orthogonal velocity component, it is the transport velocity in the generic peripheral direction. By comparing the source terms of the momentum equation in terms of the body-centered peripheral velocity component, $\xi$, and using the argument that at high Dean number flows, the axial pressure gradient becomes proportional to the square root of Dn, one can arrive at a new flow transition group $\gamma = Gn/Dn^{3/2} = \eta(\lambda Dn)^{-1/2}$. When $\gamma > 0.2$, the flow is one-vortex type (or swirl-like) when viewed in the generic coordinate system. When $\gamma < 0.2$, the flow is two-vortex type. When $\gamma \leq 0.01$, the helical flow problem can be approximated by a toroidal flow (Dean) problem (Liu and Masliyah, 1993b).

Steady developing flows in a helical pipe of finite pitch were studied by Liu (1992) and Liu and Masliyah (1993c). They qualified the use of the parabolized equations and obtained some new results on the developing flow behavior. They found that when the torsion is dominant, the flow in helical pipes tends to be the same as that in a straight pipe. When torsion is small, the developing flow is oscillatory and develops more quickly than that in a straight pipe.

There are no literature studies on developing heat transfer in helical pipes that have a finite pitch. It is interesting to note that simultaneous developing flow and heat transfer with a uniform constant temperature have not been studied as yet for the case of a torus.

In this paper, the Separation Method (Liu 1992; Liu and Masliyah 1993a) is used to solve the simultaneous developing laminar flow and forced-convective heat transfer problem in helical pipes of a finite pitch. The coordinate system used is the one first introduced by Germano (1982).

## 2. Governing equations

Figure 1 shows a sketch of a helical coil and its relevant reference coordinate systems and parameters. It can be shown that a helical system can be established in reference to the

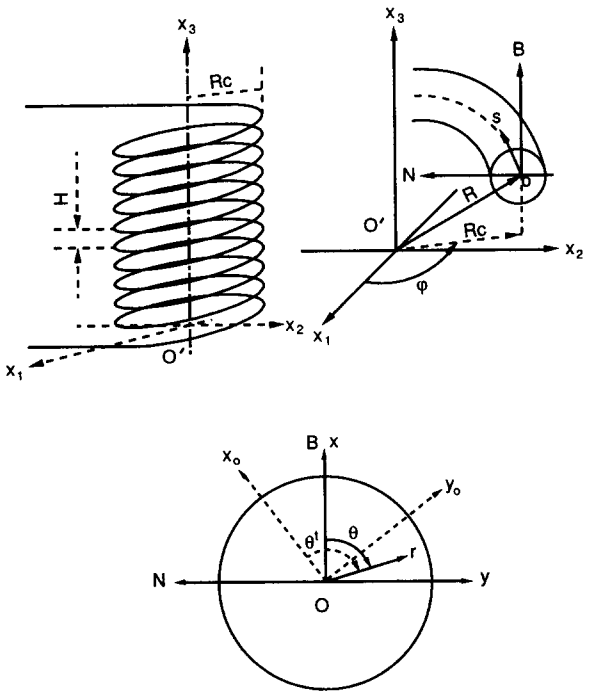


*Figure 1* Helical coil system setup

master Cartesian coordinate system $\vec{x}$ $(x_1, x_2, x_3)$. The local vectors $(\vec{N}, \vec{B}, \vec{T})$ originated on the generic curve of the helix can be mapped correspondingly to the master Cartesian coordinate system (Liu, 1992) by

$$\vec{R} = (R_c \cos\varphi, R_c \sin\varphi, bs) \tag{1}$$

$$\vec{T} = \frac{d\vec{R}}{ds} = (-\lambda^{1/2} R_c^{1/2} \sin\varphi, \lambda^{1/2} R_c^{1/2} \cos\varphi, b) \tag{2}$$

$$\vec{N} = \frac{1}{\lambda}\frac{d\vec{T}}{ds} = (-\cos\varphi, -\sin\varphi, 0) \tag{3}$$

$$\vec{B} = \vec{T} \times \vec{N} = (b \sin\varphi, -b \cos\varphi, \lambda^{1/2} R_c^{1/2}) \tag{4}$$

$$\varphi = s\left[R_c^2 + \left(\frac{H}{2\pi}\right)^2\right]^{-1/2} \tag{5}$$

where

$$b = (\eta H/2\pi)^{1/2}$$

$\vec{R}$ is the global coordinate vector at the point of consideration O on the generic curve. The generic curve is the track of a particle moving along the center of the helical pipe. $\vec{T}$ (shown as $s$ in Figure 1), $\vec{N}$, and $\vec{B}$ are the tangential, normal, and binormal to the generic curve at the point of consideration on the generic curve, respectively. Here, $s$ is the dimensionless curve length parameter along the generic curve, $s = s'/a$. The orthogonality of a helical coordinate system can

## Notation

| | |
|---|---|
| $a$ | Radius of pipe, dimensional |
| $b$ | Torsion parameter, $(\eta H/2\pi)^{1/2}$ |
| $\vec{B}$ | Binormal |
| $C_p$ | Heat capacity, dimensional |
| Dn | Dean number, Re $\lambda^{1/2}$ |
| $d_\phi$ | Extra diagonal term |
| $f$ | Fanning friction factor |
| $f(s)$ | Function of $s$ |
| $g$ | Matric coefficient |
| Gn | Germano number, Re $\eta$ |
| $H$ | Pitch |
| $h$ | Heat transfer coefficient, dimensional |
| $\bar{h}$ | Average heat transfer coefficient |
| $h_i$ | $i$-coordinate metrics |
| $i, j$ | Index |
| $k$ | Thermal conductivity, dimensional |
| $L_{Nu}$ | Thermal developing length |
| $M$ | Momentum operator |
| $\vec{N}$ | Normal |
| Nu | Nusselt number |
| $O$ | Origin |
| $p$ | Pressure |
| Pe | Peclet number |
| Pr | Prandtl number |
| $q$ | Heat flux, dimensional |
| $q_i$ | $i$-coordinate |
| $R_c$ | Radius of coil |
| Re | Reynolds number |
| $r$ | Radial coordinate |
| $S_\phi$ | Source term |
| $s$ | Axial coordinate |
| $s^+$ | $s$/2Re |
| $T$ | Temperature |
| $\vec{T}$ | Tangential |
| $t$ | Time |
| $x_1, x_2, x_3$ | Cartesian coordinates |
| $U$ | Average axial velocity, dimensional |
| $u, u_1$ | Axial velocity |
| $v$ | Radial velocity |
| $w, u_3$ | Orthogonal peripheral velocity |

*Greek symbols*

| | |
|---|---|
| $\gamma$ | Flow pattern transition parameter |
| $\eta$ | Torsion |
| $\theta$ | Nonorthogonal peripheral coordinate |
| $\theta'$ | Orthogonal peripheral coordinate |
| $\lambda$ | Curvature ratio |
| $\mu$ | Dynamic viscosity, dimensional |
| $\nu$ | Kinematic viscosity, dimensional |
| $\xi$ | Nonorthogonal peripheral velocity |
| $\rho$ | Density, dimensional |
| $\varphi$ | Angle |
| $\phi$ | Physical variable |
| $\psi$ | Pseudo-stream function |

*Subscripts*

| | |
|---|---|
| av | Average |
| c | Normalized |
| fd | Fully developed |
| b | Bulk |
| $i, j, k$ | Index |
| o | Orthogonal |
| w | Wall |
| 1, 2, 3 | Index |

*Superscript*

| | |
|---|---|
| ' | Dimensional quantity |

be achieved by rotating the bases formed by the Frenet frame $\vec{B}$ and $\vec{N}$ around the $s$ axis.

A given point in the pipe $(s, r, \theta)$ can be mapped to the master Cartesian system $(x_1, x_2, x_3)$ through the following equation:

$$\vec{x} = \vec{R} + r\cos\theta\vec{N} + r\sin\theta\vec{B} \tag{6}$$

The metrics for the transformation are given by

$$g_{ij} = \frac{\partial x_k}{\partial q_i}\cdot\frac{\partial x_k}{\partial q_j} \tag{7}$$

where $q_1 = s, q_2 = r, q_3 = \theta^t$, and $\theta^t = \theta + f(s)$. The basic equations of the curve theory

$$\frac{d\vec{N}}{ds} = \eta\vec{B} - \lambda\vec{T} \tag{8}$$

and

$$\frac{d\vec{B}}{ds} = -\eta\vec{N} \tag{9}$$

can be applied to derive the metrics of the orthogonal helical system. The curvature ratio is defined by

$$\lambda = \frac{R_c}{R_c^2 + (H/2\pi)^2} \tag{10}$$

and the torsion is

$$\eta = \frac{(H/2\pi)}{R_c^2 + (H/2\pi)^2} \tag{11}$$

By forcing $g_{ij} = 0$, for $i \neq j$, $i, j = 1, 2, 3$, with a suitable choice on the function of $f(s)$, the helical coordinate system $(s, r, \theta^t)$ is set to be orthogonal. The metrics for the coordinate system can be obtained as

$$\begin{cases} h_1 = g_{11}^{1/2} = 1 + \lambda r\sin\theta \\ h_2 = g_{22}^{1/2} = 1 \\ h_3 = g_{33}^{1/2} = r \end{cases} \tag{12}$$

where $\theta^t = \theta + \eta s$. As shown in Figure 1, the cylindrical helical coordinate system $(s, r, \theta^t)$ and the rectangular helical coordinate system $(s, x_0, y_0)$ are orthogonal. Both orthogonal $(s, r, \theta^t)$ and nonorthogonal $(s, r, \theta)$ coordinates share the same cross section.

The governing equations are first derived in the orthogonal system $(s, r, \theta^t)$ and transformed to the nonorthogonal system $(s, r, \theta)$, leaving the velocity components untouched. The transformation is necessary to eliminate the $s$-dependent coefficients and variable $(\theta^t - \eta s)$, which always appears in place of $\theta$. This allows an axially invariant solution to be realizable. Variables are nondimensionalized in the following manner:

$$s = \frac{s'}{a},\ r = \frac{r'}{a},\ t = \frac{vt'}{a^2},\ u = \frac{u'}{2U},\ v = \frac{v'}{2U},\ w = \frac{w'}{2U},\ p = \frac{\mathrm{Re}\,p'}{4\rho U^2}$$

and

$$R_c = \frac{R_c'}{a},\ H = \frac{H'}{a},\ \mathrm{Re} = \frac{2aU}{\nu},\ \mathrm{Pr} = \frac{\mu C_p}{k},\ T = \frac{T' - T_w'}{T_b' - T_w'}$$

The final governing flow equations after the necessary substitution and rearrangement are shown as follows.

The continuity,

$$\frac{1}{h_1}\left(\frac{\partial u}{\partial s} - \eta\frac{\partial u}{\partial\theta}\right) + \frac{1}{rh_1}\frac{\partial(rh_1 v)}{\partial r} + \frac{1}{rh_1}\frac{\partial(h_1 w)}{\partial\theta} = 0 \tag{13}$$

where $h_1$ is the metric coefficient in the axial direction ($s$-direction).

$$h_1 = 1 + \lambda r\sin\theta \tag{14}$$

The momentum and energy equations are given in the following form:

$$(M + d_\phi)\phi = S_\phi \tag{15a}$$

where the momentum or energy operator $M$ is defined by

$$M\phi = \frac{\partial\phi}{\partial t} + \frac{2\eta}{h_1^2}\frac{\partial^2\phi}{\partial s\,\partial\theta} + \frac{1}{h_1}\frac{\partial}{\partial s}\left[\left(\mathrm{Re}\,u - \lambda\eta r\frac{\cos\theta}{h_1^2}\right)\phi - \frac{1}{h_1}\frac{\partial\phi}{\partial s}\right] + \frac{1}{rh_1}\frac{\partial}{\partial r}\left[rh_1\left(\mathrm{Re}\,v\phi - \frac{\partial\phi}{\partial r}\right)\right] + \frac{1}{rh_1}\frac{\partial}{\partial\theta}\left[\mathrm{Re}\,(h_1 w - \eta r u)\phi - \frac{h_1}{r}\left(1 + \frac{\eta^2 r^2}{h_1^2}\right)\frac{\partial\phi}{\partial\theta}\right] \tag{15b}$$

$\phi$ stands for any velocity component or the temperature. When $\phi = T$, the Reynolds number Re in Equation 15b is replaced by Pr Re. The individual momentum and energy equations are obtained by a specification of the velocity component or the temperature $\phi$, an extra diagonal term $d_\phi$ and the source term $S_\phi$.

$s$-momentum: $\phi = u$

$$d_\phi = \frac{v\sin\theta + w\cos\theta}{h_1}\lambda\,\mathrm{Re} + \frac{\lambda^2}{h_1^2} \tag{16a}$$

$$S_\phi = -\frac{1}{h_1}\left(\frac{\partial p}{\partial s} - \eta\frac{\partial p}{\partial\theta}\right) + \frac{2\lambda}{h_1^2}\left[\sin\theta\left(\frac{\partial v}{\partial s} - \eta\frac{\partial v}{\partial\theta}\right) + \cos\theta\left(\frac{\partial w}{\partial s} - \eta\frac{\partial w}{\partial\theta}\right)\right] + \frac{\lambda\eta}{h_1^3}[\cos\theta v - (\lambda r + \sin\theta)w] \tag{16b}$$

$r$-momentum: $\phi = v$

$$d_\phi = \frac{1 + 2h_1\lambda r\sin\theta}{r^2 h_1^2} \tag{17a}$$

$$S_\phi = -\frac{\partial p}{\partial r} + \mathrm{Re}\left(\frac{\lambda\sin\theta}{h_1}u^2 + \frac{w^2}{r}\right) - \frac{2\lambda\sin\theta}{h_1^2}\left(\frac{\partial u}{\partial s} - \eta\frac{\partial u}{\partial\theta}\right) + \frac{\lambda\eta\cos\theta}{h_1^3}u - \frac{2}{r^2}\frac{\partial w}{\partial\theta} - \frac{2h_1 - 1}{rh_1^2}\lambda\cos\theta w \tag{17b}$$

$\theta$-momentum: $\phi = w$

$$d_\phi = \mathrm{Re}\frac{v}{r} + \frac{1}{h_1^2}\left(\lambda^2 + \frac{2h_1 - 1}{r}\right) \tag{18a}$$

$$S_\phi = -\frac{\partial p}{\partial\theta} + \mathrm{Re}\frac{\lambda\cos\theta}{h_1}u^2 - \frac{2\lambda\cos\theta}{h_1^2}\left(\frac{\partial u}{\partial s} - \eta\frac{\partial u}{\partial\theta}\right) - \frac{\lambda r + \sin\theta}{h_1^2}\lambda\eta u + \frac{3h_1 - 1}{r^2 h_1^2}\frac{\partial v}{\partial\theta} + \frac{\lambda\cos\theta}{rh_1^2}v \tag{18b}$$

With the assumption that the viscous dissipation is negligible and the fluid is incompressible with constant physical properties, the energy equation can be written as

$$\phi = T,\quad d_\phi = 0,\quad S_\phi = 0 \tag{19}$$

where the Reynolds number Re is replaced by the Peclet number Pe = Pr Re in Equation 15b.

The physical boundary is defined by the pipe wall. Although a numerical scheme with a cylindrical coordinate system would normally have a condition set at the center of the pipe, the

centerline of the pipe is simply in the interior of the computational domain and does not need to be treated differently. The boundary and necessary conditions are

$$u = v = w = T = 0 \qquad \text{at } r = 1 \text{ for all } s \text{ and } \theta$$

$p = 0$ at one reference point inside the computational domain and

$$\frac{\int_0^{2\pi} d\theta \int_0^1 ru\, dr}{\pi} = \frac{1}{2} \quad \text{(from the nondimensionalization)} \tag{20}$$

The inlet conditions for the flow and the temperature fields are given by

$$\begin{cases} v|_{s=0} = w|_{s=0} = 0 \\ \left.\dfrac{\partial p}{\partial r}\right|_{s=0} = \left.\dfrac{\partial p}{\partial \theta}\right|_{s=0} = 0 \\ T|_{s=0} = 1 \end{cases} \tag{21}$$

for $0 \le r \le 1$ and $0 \le \theta \le 2\pi$.

Two inlet axial flow conditions will be investigated. These are referred to as Parabolic axial velocity entry:

$$u|_{s=0} = 1 - r^2 \tag{22}$$

Uniform axial velocity entry:

$$u|_{s=0} = \frac{1}{2} \tag{23}$$

The parabolic axial velocity entry defined by Equation 22 together with Equation 21 corresponds to a flow having passed through a long straight pipe prior to entering the helical pipe. The uniform axial velocity entry defined by Equation 23 together with Equation 21 are valid for a flow entering a helical pipe from a large reservoir.

When the flow reaches the fully developed (i.e., axially invariant) stage, the (generic) transverse velocity field $(v, \xi)$ can be represented by a field potential, $\psi$, as follows:

$$rh_1 v = -\frac{\partial \psi}{\partial \theta} \tag{24a}$$

$$h_1 \xi = h_1 w - \eta r u = \frac{\partial \psi}{\partial r} \tag{24b}$$

where $\xi$ is the body-centered peripheral velocity component. $\xi$ is not an orthogonal velocity component, but does indicate the flow and transfer rate in the $\theta$-direction.

To the same extent as for two-dimensional (2-D) flows, the potential $\psi$ can be called the (pseudo-) secondary flow-stream function. To compute the secondary flow-stream function, Equation 24b can be used after the velocity field is obtained. The pseudo-secondary flow-stream function was first introduced by Wang (1981) and was subsequently used by Germano (1982, 1989), Tuttle (1990), Xie (1990), and Liu and Masliyah (1993b, c). However, Germano (1982, 1989) and Xie (1990) considered that $\psi$ is not a good choice for the purpose of representing the secondary flow. Tuttle (1990) and Liu and Masliyah (1993b) preferred to use $\psi$ instead of the orthogonal velocity vectors.

In an attempt to seek a more suitable representation, Xie (1990) followed the approach of Murata et al. (1981) by utilizing the nonorthogonal coordinate system. Based on the nonorthogonal base vectors of the plane $(\vec{r}, \vec{\theta})$, he argued that one can form an "orthogonal engineering coordinate system" using the base vectors $(\vec{r}, \vec{\theta}, \vec{r} \times \vec{\theta})$. Having the same base vectors on the cross-sectional plane, the "engineering coordinate system" and the original Frenet frame should not be different in property, based on Equations 2–4. The pseudo-stream function given by Xie (1990) corresponds to our pseudo-secondary flow-stream function when $\lambda$ is negligibly small. However, his "stream function" $\psi^*$ based on the "engineering coordinate system" does not have stream-function properties, since its use does not satisfy the continuity equation. Moreover, for a torus, i.e., zero torsion, $\psi^*$ reduces to $\psi^* = \int_r^1 rw\, dr$. Hence $\psi^*$ is not a proper choice for describing the helical flow.

The experimental observations by Liou (1992) are a definite support for using the pseudo-secondary flow-stream function. His flow visualization was favorably compared with the results of Wang (1981) and Chen and Fan (1986), which were based on the nonorthogonal coordinate system. Liou's results for the flow pattern transition showed very good agreement with those predicted by Liu (1992) and Liu and Masliyah (1993b) for small Dean number flows.

The normalized axial pressure gradient is directly related to the friction factor as follows:

$$f\,\mathrm{Re} = \frac{4 \int_0^1 r\, dr \int_0^{2\pi} \left(-\dfrac{\partial p}{\partial s}\right) d\theta}{\pi} \tag{25}$$

From the governing equations (Equations 13 through 19), it can be seen that the controlling parameters are Pr, Re, $\lambda$, and $\eta$. However, it is more convenient to work with the fluid Prandtl number Pr, Dean number Dn, curvature ratio $\lambda$ and Germano number Gn. For the special case of large Dean number flows, the flow-pattern transition parameter $\gamma$ can be used instead of Gn. The dimensionless groups are summarized below:

$$\mathrm{Pr} = \frac{\mu C_p}{k} \tag{26}$$

$$\mathrm{Dn} = \mathrm{Re}\,\lambda^{1/2} = \mathrm{Re}\left[\frac{R_c}{R_c^2 + (H/2\pi)^2}\right]^{-1/2} \tag{27}$$

$$\mathrm{Gn} = \mathrm{Re}\,\eta = \mathrm{Re}\,\frac{H/2\pi}{R_c^2 + (H/2\pi)^2} \tag{28}$$

$$\gamma = \mathrm{Gn}\,\mathrm{Dn}^{-3/2} = \eta(\lambda\,\mathrm{Dn})^{-1/2} \tag{29}$$

$\gamma$ and $\eta$ are given by Equations 10 and 11, respectively.

When loose coiling approximation is invoked, i.e., $\lambda \to 0$, forced convective heat transfer in a helical pipe becomes governed by Pr, Dn and Gn, or $\gamma$. Consequently, for a torus, (Gn = 0) with small curvature ratio, Pr and Dn become the two controlling parameters.

The normalized axial length $s^+$ is used to present the flow and heat transfer development. It is defined by

$$s^+ = \frac{s'}{2a\,\mathrm{Re}} = \frac{s}{2\,\mathrm{Re}} \tag{30}$$

To show the peripheral distribution of the heat transfer coefficient, a local Nusselt number is defined as follows:

$$\mathrm{Nu}(\theta) = \frac{2ah}{k} = -\frac{2}{T_{av}} \left.\frac{\partial T}{\partial r}\right|_{r=1} \tag{31}$$

where $h$ is the local heat transfer coefficient and $T_{av}$ is the average fluid average temperature which is defined as:

$$T_{av} = \frac{2}{\pi} \int_0^1 dr \int_0^{2\pi} ruT\, d\theta \tag{32}$$

The average Nusselt number, Nu is defined by

$$\mathrm{Nu} = \frac{2a\bar{h}}{k} = \frac{1}{2\pi} \int_0^{2\pi} (1 + \lambda \sin\theta)\,\mathrm{Nu}(\theta)\, d\theta \tag{33}$$

where $\bar{h}$ is the axially weighted peripherally averaged heat transfer coefficient and is given by

$$\bar{h} = \frac{q}{2\pi a(T'_{av} - T'_w)\Delta s'} \tag{34}$$

Here, $q$ is the heat flux and $\Delta s'$ is the pipe axial length measured along the pipe center.

For convenience, the temperature distribution across a given pipe section is normalized by its average value $T_{av}$, i.e.,

$$T^c = \frac{T}{T_{av}} \tag{35}$$

When no confusion arises, the superscript c will be dropped.

## 3. Results and discussions

Calculations were made for Dean numbers in the range of $20 \le Dn \le 5000$ for $0.1 \le Pr \le 500$, $0.01 \le \lambda \le 0.25$, and $\gamma \le 0.1$. The grid used in most cases for $Dn < 2000$ is n40 × 50fu, i.e., **40** non-uniform mesh points in the radial direction and **50** uniform mesh points in the full peripheral direction. For Dn = 2,000 and Dn = 5,000, the corresponding meshes are n60 × 50fu and n100 × 60fu, respectively.

Before we present the results for developing heat transfer, it is necessary to introduce the characterization of the fully developed laminar helical flows using the orthogonal and nonorthogonal coordinate systems. Figure 2 shows the secondary flow as represented by the two coordinate systems. Figures 2a and 2b are based on the orthogonal system, whereas Figures 2c and 2d are based on the non-orthogonal system. When torsion is large, Figures 2a and 2c show that the secondary flow patterns in the two coordinate systems are very different. From the perspective of the orthogonal system, Figure 2a shows a two-vortex structure with sources and sinks. When viewed in the nonorthogonal coordinate system, the secondary flow pattern is of a one-vortex type as shown in Figure 2c. However, when torsion is small, the secondary flow is of a normal two-vortex pattern, similar to that for a torus.

The qualitative behavior of the axial flow and the secondary flow pattern is little affected by $\lambda$, $\eta$, and Dn when $\lambda < 0.6$,

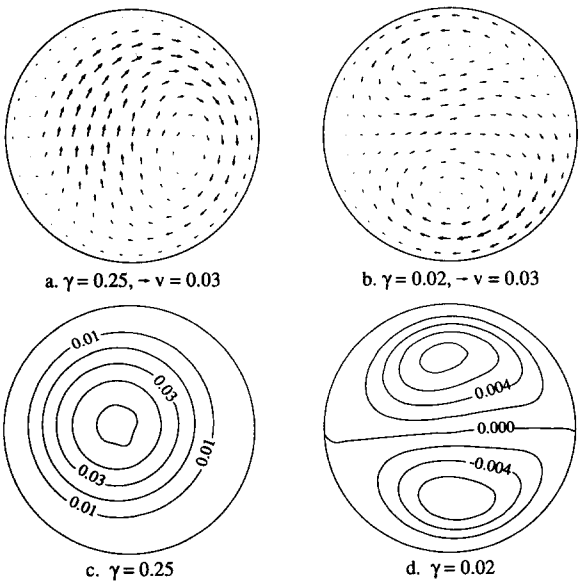


*Figure 2* Secondary flow structure variation with torsion for Dn = 100 and $\lambda = 0.01$ ($\eta = \gamma$)

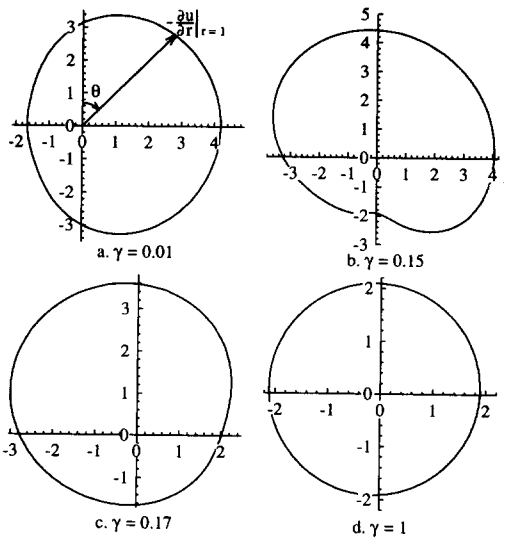


*Figure 3* The axial wall shear rates distribution variation with the torsion $\gamma$ for Dn = 100 and $\lambda = 0.01$ ($\eta = \gamma$)

$\gamma \le 0.01$ for $Dn \ge 50$. The torsion effect on the flow is noticeable when $\gamma > 0.01$. Figure 3 shows the effect of torsion on the axial wall shear rate $-\left.\frac{\partial u}{\partial r}\right|_{r=1}$. As shown in Figure 3a, the values of the axial wall shear rate is the polar distance from the origin of the plot, and $\theta$ is the nonorthogonal peripheral coordinate. Figures 3a to 3c show the peripheral variation of the shear rate when the flow is a two-vortex type. On the other hand, Figure 3d shows the variation for a one-vortex type flow. In the former case, the shear-rate peripheral variation is strongly dependent on $\gamma$, whereas for the latter case, it is not dependent on $\gamma$.

We shall now discuss developing heat transfer corresponding to both one- and two-vortex flows.

### 3.1. Heat transfer Nusselt number development

Owing to the substantial magnitude of the secondary flow and to its oscillatory development (Liu 1992), the temperature profile and the Nusselt number are not expected to be monotonic (although they may not be regularly cyclic) in the course of the development along the axial direction. This oscillatory behavior was also observed experimentally (see Janssen and Hoogendoorn 1978). However, for a fully developed flow in a torus, periodic oscillation in the Nusselt number was found in the analysis of developing heat transfer by Tarbell and Samuels (1973).

Figures 4 and 5 show the Nusselt number development for a torus having $\lambda = 1/41$ for various Prandtl numbers. The oscillation in Nusselt number is evident even for the small Dean number, Dn = 21.86, and small Prandtl number, Pr = 0.707, a case shown in Figure 4. For comparison purposes, the experimental data by Janssen and Hoogendoorn (1978) for the same conditions as those used in the computation are also shown in Figures 4 and 5. It can be observed that the current predictions are in good agreement with the experimental results of Janssen and Hoogendoorn (1978). It is of interest to note that the agreement is very good even for the case of small Dn flows, as shown in Figure 4.

Figures 6 and 7 show the Nusselt number development in helical pipes that have a finite pitch for different Prandtl numbers. It can be observed that in all cases, the Nusselt number varies nonmonotonically with the axial length. The

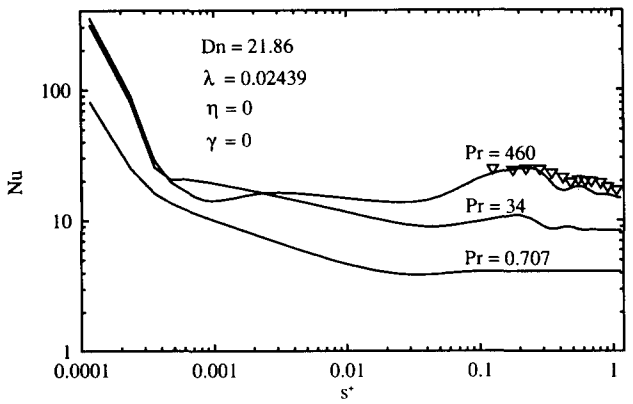


*Figure 4* Nusselt number development for a small Dn flow in torus with uniform axial velocity entry. ∇ represents the experimental data of Janssen and Hoogendoorn (1978)

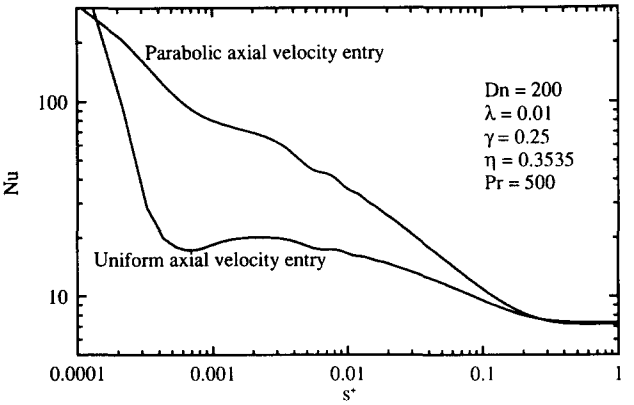


*Figure 6* Nusselt number development for a two-vortex flow with Dn = 200, $\lambda = 0.01$, and $\gamma = 0.01$ ($\eta = 0.01414$)

magnitude of the oscillation decreases with increasing axial length. The oscillations damp out as the flow becomes thermally fully developed. For very large Dn number flows, it was found that the Nusselt number development does not differ qualitatively from that of smaller Dn flows. When $\gamma < 0.2$, the heat transfer development is similar to that for a torus where two vortices are present in the secondary flow. On the other hand, when $\gamma > 0.2$, one vortex pattern appears in the secondary flow, and the heat transfer development is similar to that for a straight pipe.

Figure 8 shows the variations of the local Nusselt number at the inner wall ($\theta = -\pi/2$), the upper wall ($\theta = 0$), and the outer wall ($\theta = \pi/2$), with axial length for a typical two-vortex flow with Dn = 2000, $\lambda = 0.1$, and $\gamma = 0.001414$ for Pr = 0.707. From Figure 8, we observe that the local Nusselt number is oscillatory in the course of its development. The local maximum Nusselt number crosses over from the inner wall to the outer wall near the inlet. This behavior is very similar to that of the axial wall shear rate development (Liu 1992). The crossover points are Dn $s^+ = 0.20$ (or $s = 0.63$) for Pr = 0.707, Dn $s^+ = 0.19$ (or $s = 0.60$) for Pr = 2, and Dn $s^+ = 0.10$ (or $s = 0.32$) for Pr = 500. Figure 8 clearly shows that development of the local Nusselt number, Nu($\theta$), is sensitive to the peripheral location.

Figure 9 shows the asymptotic local Nusselt number distribution with $\theta$ for both the two- and one-vortex flows. These two plots are in polar coordinates, and Nu($\theta$) is measured by the polar distance. The horizontal and vertical lines correspond to the $y$- and $x$-axes of the nonorthogonal (generic) coordinates. Figure 9a shows the local Nusselt number variation with $\theta$ for a typical two-vortex flow of Dn = 200, $\lambda = 0.01$, and $\gamma = 0.01$, a case similar to a torus. We observe that the local Nusselt number reaches its maximum at the outer wall ($\theta = \pi/2$) and its minimum at the inner wall ($\theta = -\pi/2$). Figure 9b shows the local Nusselt number variation with $\theta$ for a typical one-vortex flow with Dn = 200, $\lambda = 0.01$, and $\gamma = 0.25$, a case similar to a straight pipe. We observe that Nu($\theta$) variation is very different from that of Figure 9a. Nu($\theta$) is higher in the region of the inner upper wall ($\theta \approx -\pi/4$) and smaller in the region of the lower outer wall ($\theta \approx 3\pi/4$). Comparing Figure 9a with Figure 9b, we observe that the local Nusselt number has a strong dependence on $\theta$ for a two-vortex flow, whereas Nu($\theta$) is relatively invariant with $\theta$ for the case of a one-vortex flow.

### 3.2. Temperature field

The temperature distribution depends on the flow Dean number, the flow pattern transition parameter, and the fluid Prandtl number. Figure 10 shows the temperature distribution for various Pr for a fixed pipe geometry and flow Dean number. Figures 10a to 10c clearly indicate that the temperature profiles are strongly dependent on the fluid Prandtl number. When Pr = 0.01, Figure 10a shows a temperature profile similar to

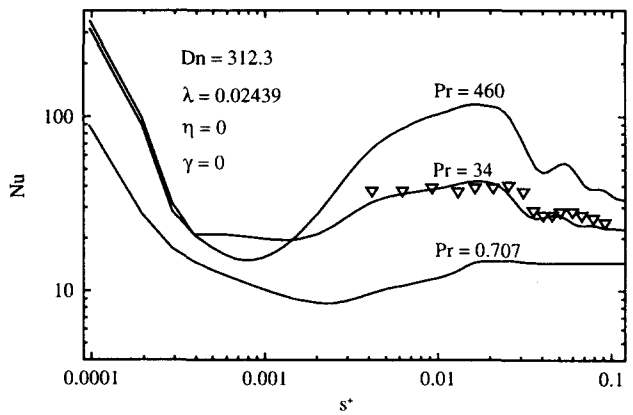


*Figure 5* Nusselt number of development for Dn = 312.3 in a torus with uniform axial velocity entry. ∇ represents the experimental data of Janssen and Hoogendoorn (1978)

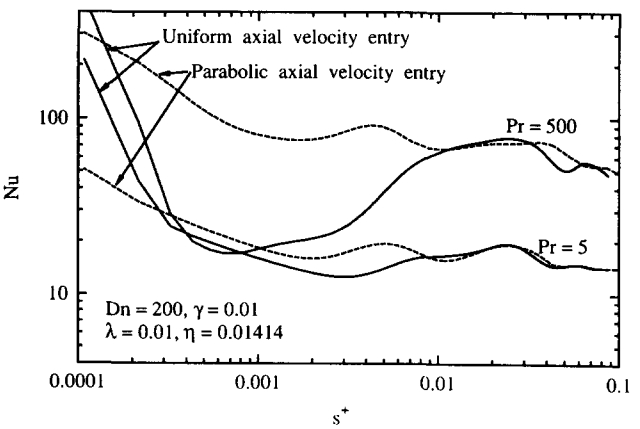


*Figure 7* Nusselt number development for a one-vortex flow with Dn = 200, $\lambda = 0.01$, and $\gamma = 0.25$ ($\eta = 0.3535$)

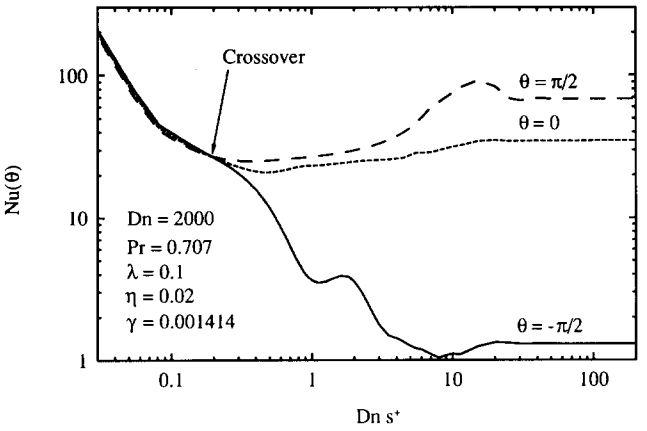


*Figure 8* Local Nusselt number development for a typical two-vortex flow with Dn = 2000, $\lambda = 0.1$, and $\gamma = 0.001414$ for Pr = 0.707. Uniform axial velocity entry

that in a straight pipe. For the case of Pr = 1, Figure 10b shows a temperature profile similar to the velocity profile shown in Figure 10d. When the fluid Prandtl number is large, Pr = 100, Figure 10c shows that the temperature profile splits into two parts at the vortex dividing line where a depression zone is found. When torsion is dominant, i.e., a one-vortex flow is present, the temperature profile does not split in the center region, and it is similar to that for a straight pipe.

### 3.3 Thermal developing length and asymptotic Nusselt numbers

The thermal developing length, $L_{Nu}$, is defined as the length at which the peripherally averaged Nusselt number varies within 1 percent of the fully developed peripherally averaged Nusselt number. That is,

$$L_{Nu} = s^+|_{|Nu-(Nu)_{fd}| \le 0.01(Nu)_{fd}} \tag{36}$$

Some computed values of Nu and the thermal developing length are listed in Table 1 for the case of helical flow with a uniform axial velocity entry. The fully developed (asymptotic) values are listed without the fd subscript. The use of the subscript fd in Equation 36 is only for the purpose of avoiding confusion with the local values.

Table 1 indicates that the thermal developing length is a function of the flow Dean number, the fluid Prandtl number, and the coil geometrical parameters $\eta$ and $\lambda$. For fixed Pr, $\lambda$, and $\eta$, the thermal developing length is a strong function of the flow Dean number, where $L_{Nu}$ decreases with Dn. Also, there

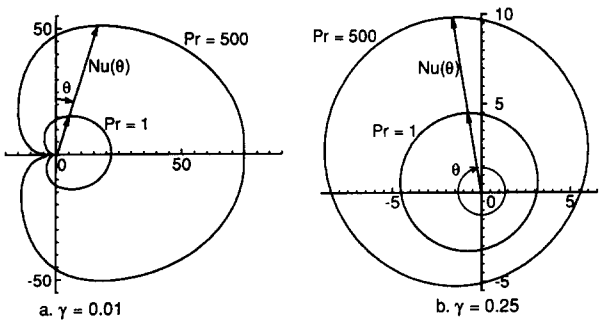


*Figure 9* Fully developed Nu($\theta$) variation with $\theta$ for Dn = 200 and $\lambda = 0.01$

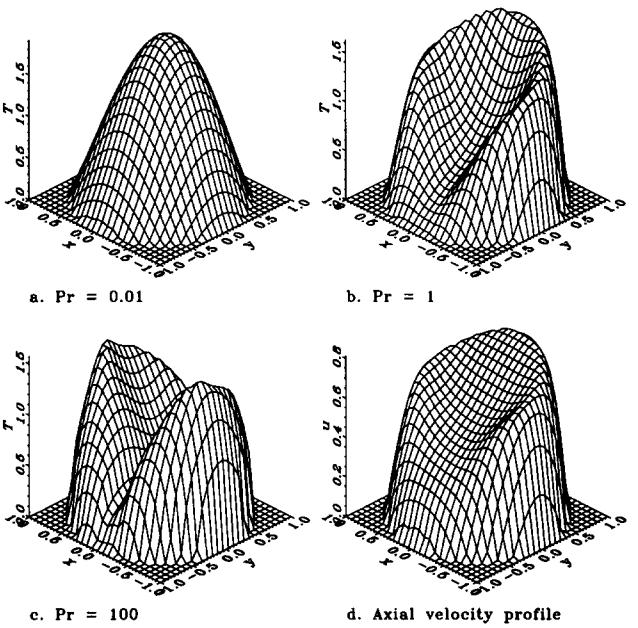


*Figure 10* Developed temperature profiles for various Pr values together with the axial velocity profile for a typical two-vortex flow with Dn = 200, $\lambda = 0.1$, and $\eta = 0.05$ (or $\gamma = 0.01118$)

is a large dependence of $L_{Nu}$ on Pr with the other parameters being fixed. Here $L_{Nu}$ increases with Pr. The dependence of $L_{Nu}$ on $\lambda$ and $\eta$ is to a large extent a weak one. For example, for Dn = 100 for $\lambda = 0.1$, a change in $\eta$ from 0.05 to 0.15 gives a variation in $L_{Nu}$ of about 20 percent. Here the flow pattern remains that of a two-vortex type. Similarly, for Dn = 200 and $\lambda = 0.1$, Table 1 indicates a very slight variation in $L_{Nu}$ with $\eta$, especially for Pr = 1. Once again the flow remains a two-vortex type. However, there is a large variation of $L_{Nu}$ when considering Dn = 200 and $\lambda = 0.01$ for $\eta = 0.014$ to 0.354. This abrupt change in $L_{Nu}$ is due to the change in the flow pattern. For $\eta = 0.014$ and 0.028, the flow has a two-vortex pattern, whereas for $\gamma = 0.283$ and 0.354 the flow has a one-vortex pattern. To show more clearly the thermal-developing-length variation with torsion a plot of $L_{Nu}$ versus $\gamma$ for the case of Dn = 100 and $\lambda = 0.0025$ ($\eta = 0.5\gamma$) is shown in Figure 11. It can be observed that $L_{Nu}$ is strongly dependent on $\gamma$ in the vortex transition region ($0.1 < \gamma < 0.3$); otherwise, the developing length increases with increasing torsion quite smoothly.

We correlated the computed thermal developing length by neglecting $\lambda$ and $\eta$ effects for $\eta \le \lambda$ pipes. The thermal developing length is a function of both Dn and Pr. Our results can be represented by

$$L_{Nu} = \frac{0.155 + 0.00604\,\mathrm{Dn}^{1/2}\,\mathrm{Pr}^{1/4}}{1 + 0.0122\,\mathrm{Dn}\,\mathrm{Pr}}\,\mathrm{Pr} \tag{37}$$

for $0.01 \le \lambda \le 0.15$, $\eta \le \lambda$, $20 \le \mathrm{Dn} \le 5000$ and $0.1 \le \mathrm{Pr} \le 500$.

Janssen and Hoogendoorn (1978) gave a bound estimate on $L_{Nu}$ as

$$L_{Nu} \le \frac{20\,\mathrm{Pr}^{0.2}}{\mathrm{Dn}} \tag{38}$$

The above bound is in agreement with the $L_{Nu}$ correlation given by Equation 37.

From Table 1, one can also observe that similar to the thermal developing length, the asymptotic Nusselt number is also strongly dependent on the flow Dean and Prandtl numbers. The asymptotic Nusselt number is little affected by

**Table 1.** Developing lengths and asymptotic Nu values for uniform axial velocity entry

| Dn | $\lambda$ | $\eta$ | Pr | Nu | $L_{Nu}$ | Pr | Nu | $L_{Nu}$ | Pr | Nu | $L_{Nu}$ |
|---|---|---|---|---|---|---|---|---|---|---|---|
| 21.86 | 0.024 | 0 | 0.707 | 4.01 | 0.0803 | 34 | 8.455 | 0.776 | 460 | 14.8 | 1.07 |
| 91.47 | 0.143 | 0 | 0.1 | 4.590 | 0.0275 | 5 | 10.15 | 0.109 | 80 | 15.52 | 0.362 |
| 100 | 0.1 | 0 | | | | 1 | 8.694 | 0.0522 | | | |
| 100 | 0.1 | 0.05 | | | | 1 | 8.688 | 0.0513 | | | |
| 100 | 0.1 | 0.1 | | | | 1 | 8.675 | 0.0470 | | | |
| 100 | 0.1 | 0.15 | | | | 1 | 8.651 | 0.0412 | | | |
| 182.9 | 0.143 | 0 | 0.1 | 5.186 | 0.0224 | 5 | 14.02 | 0.0746 | | | |
| 200 | 0.01 | 0.014 | 0.1 | 5.224 | 0.0215 | 5 | 14.35 | 0.0691 | | | |
| 200 | 0.01 | 0.028 | 0.1 | 5.260 | 0.0235 | 5 | 14.38 | 0.0691 | | | |
| 200 | 0.01 | 0.283 | 0.1 | 3.738 | 0.0343 | 5 | 4.569 | 0.1088 | | | |
| 200 | 0.01 | 0.354 | 0.707 | 3.74 | 0.0422 | 2 | 3.923 | 0.0868 | 500 | 7.189 | 0.391 |
| 200 | 0.1 | 0 | | | | 1 | 12.27 | 0.0399 | 100 | 25.5 | 0.0905 |
| 200 | 0.1 | 0.05 | | | | 1 | 12.03 | 0.0398 | 100 | 27.8 | 0.0950 |
| 200 | 0.1 | 0.1 | | | | 1 | 12.30 | 0.0390 | 100 | 28.04 | 0.102 |
| 200 | 0.1 | 0.15 | | | | 1 | 12.29 | 0.0380 | 100 | 25.52 | 0.105 |
| 200 | 0.1 | 0.2 | | | | 1 | 12.32 | 0.0376 | | | |
| 200 | 0.1 | 0.3 | | | | 1 | 12.30 | 0.0398 | | | |
| 312.3 | 0.024 | 0 | 0.707 | 14.6 | 0.0328 | 34 | 22.33 | 0.123 | 460 | 30.25 | 0.214 |
| 643 | 0.143 | 0 | 0.1 | 6.910 | 0.0154 | 2 | 23.00 | 0.034 | 5 | 24.67 | 0.0482 |
| 680.3 | 0.143 | 0 | 0.707 | 20.1 | 0.0276 | 4 | 25.15 | 0.0342 | 10 | 27.00 | 0.0527 |
| 721.7 | 0.083 | 0 | 0.707 | 21.9 | 0.0269 | 43 | 30.61 | 0.0883 | 500 | 50.2 | 0.1294 |
| 2000 | 0.1 | 0.02 | 0.1 | 11.26 | 0.0112 | 1 | 37.74 | 0.0186 | 100 | 63.9 | 0.0485 |
| 5000 | 0.1 | 0.02 | 0.1 | 20.25 | 0.0115 | 2 | 62.85 | 0.0137 | 500 | 123.0 | 0.0358 |

curvature ratio and torsion. A more complete picture of the asymptotic Nusselt number variation with torsion can be observed in Figure 12. In the flow-pattern transition region ($0.1 < \gamma < 0.3$), the Nusselt number varies strongly with $\gamma$. However, once the flow is a one-vortex type, the Nusselt number varies little with $\gamma$ for all values of Pr studied. For very large Pr, Nu increases rapidly with torsion for $\gamma < 0.02$.

For small torsion, $\eta \leq \lambda$, we find that our predicted asymptotic Nu is in agreement with the correlation of Manlapaz and Churchill (1981) and only for $80 < \mathrm{Dn} < 400$ and large Pr cases. The correlation due to Manlapaz and Churchill (1981) is given by

$$\mathrm{Nu} = \left\{1.158\left(\frac{\mathrm{Pr\,Dn}}{\mathrm{Pr} + 0.477}\right)^{3/2} + \left[3.657 + 4.343\left(1 + \frac{957}{\mathrm{Dn^2\,Pr}}\right)^{-2}\right]^3\right\}^{1/3} \tag{39}$$

For small Pr cases, the Nu values obtained from this study are substantially lower than that predicted by Equation 39. For Dn = 200, Pr = 0.1, Equation 39 overpredicts Nu by 50 percent. When Dn is small, Equation 39 predicts Nu very poorly as well. For example, at Dn = 21.86 and Pr = 460, Equation 39 underpredicts Nu by 75 percent. However, our results are consistent with those of Akiyama and Cheng (1972), Tarbell and Samuels (1973), and Kalb and Seader (1974). In the range of $20 \leq \mathrm{Dn} \leq 5000$, $0.1 \leq \mathrm{Pr} \leq 500$ and $\eta \leq \lambda < 0.15$, the asymptotic Nusselt number can be represented by the following equation:

$$\mathrm{Nu} = 3.657 + \frac{(0.75\,\mathrm{Dn}^{1/2} + 0.0028\,\mathrm{Pr})\,\mathrm{Pr}^{1/8}}{(1 + 0.00174\,\mathrm{Pr}^{-3})(1 + 70.6\,\mathrm{Pr}^{-0.6}/\mathrm{Dn})} \tag{40}$$

## 4. Conclusions

Simultaneous hydrodynamic and thermal development of laminar flow in a helical pipe with a finite pitch was studied. Numerical simulations using parabolized formulation show

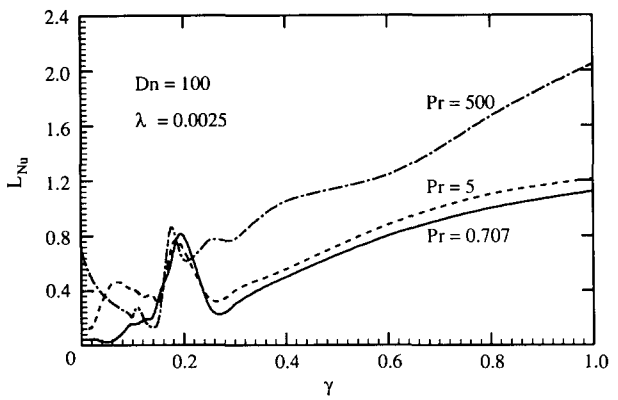


*Figure 11* Thermal developing length variation with $\gamma$ for Dn = 100 and $\lambda = 0.0025$ ($\eta = 0.5\gamma$). Uniform axial velocity entry

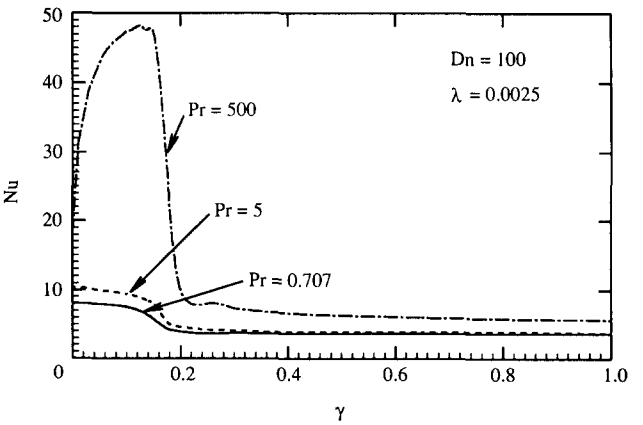


*Figure 12* Asymptotic Nusselt number variation with $\gamma$ for Dn = 100 and $\lambda = 0.0025$ ($\eta = 0.5\gamma$)

good agreement for the Nusselt number development for the limiting case of a torus. It is observed that the local maximum Nusselt number crosses over from the inner wall to the outer wall in the course of its development for small $\gamma$ flows. The thermal developing length is correlated with Pr and Dn when the effect of $\lambda$ and $\eta$ can be neglected. The fully developed (or asymptotic) Nu is found to be in good agreement with published data.

The thermal entrance length and asymptotic Nusselt number show strong dependence on $\gamma$ for $0.1 < \gamma < 0.3$. When torsion is dominant ($\gamma > 0.2$) all the heat transfer characteristics tend to the limits corresponding to those of a Poiseuille flow. When torsion is small ($\gamma < 0.2$), all the thermal characteristics are similar to those of a torus.

## Acknowledgments

The authors wish to thank the National Sciences and Engineering Research Council of Canada for financial support.

## References

Akiyama, M. and Cheng, K. C. 1972. Laminar forced convection heat transfer in curved pipes with uniform wall temperature. *Int. J. Heat Mass Transfer*, **15**, 1426–1431

Akiyama, M. and Cheng, K. C. 1974a. Laminar forced convection in the thermal entrance region of curved pipes with uniform wall temperature. *Can. J. Chem. Eng.*, **52**, 234–240

Akiyama, M. and Cheng, K. C. 1974b. Graetz problem in curved pipes with uniform wall heat flux. *Appl. Sci. Res.*, **29**, 401–418

Balejova, M., Cakrt, J., and Mik, V. 1977. Heat transfer for laminar flow in curved pipes with uniform wall heat flux. *Acta Technica Csav*, **22**, 183–194

Berger, S. A. 1991. Flow and heat transfer in curved pipes and tubes. AIAA 91-0030, 29th Aerospace Sciences Meeting, Reno, NV

Berger, S. A., Talbot, L., and Yao, L. S. 1983. Flow in curved pipes. *Annu. Rev. Fluid Mech.*, **15**, 461–512

Chen, W. H. and Fan, C. N. 1986. Finite element analysis of incompressible viscous flow in helical pipe. *Computational Mech.*, **1**, 281–292

Dravid, A. N., Smith, K. A., Merrill, E. W., and Brian, P. L. T. 1971. Effect of secondary fluid motion on laminar flow heat transfer in helically coiled tubes. *AIChE J.*, **17**, 1114–1122

Germano, M. 1982. On the effect of the torsion in a helical pipe flow. *J. Fluid Mech.*, **125**, 1–8

Germano, M. 1989. The Dean equations extended to a helical pipe flow. *J. Fluid Mech.*, **203**, 289–305

Ito, K. 1987. Flow in curved pipes. *JSME Int. J.*, **30**(262), 543–552

Janssen, L. A. and Hoogendoorn, C. J. 1978. Laminar convective heat transfer in helical coiled tubes. *Int. J. Heat Mass Transfer*, **21**, 1197–1206

Kalb, C. E. and Seader, J. D. 1974. Fully-developed viscous-flow heat transfer in curved circular tubes with uniform wall temperature. *AIChE J.*, **20**, 340–346

Liou, T. M. 1992. Flow visualization and LDV measurement of fully developed laminar flow in helically coiled tubes. *Exp. Fluids*, **13**, 332–338

Liu, S. 1992. *Laminar Flow and Heat Transfer in Helical Pipes with Finite Pitch.* Ph.D. dissertation, University of Alberta, Edmonton, Canada

Liu, S. and Masliyah, J. H. 1993a. A total decoupling numerical method for fluid flows. *Int. J. Numer. Meth. Fluids*, **16**, 659–682

Liu, S. and Masliyah, J. H. 1993b. Axially-invariant laminar flow in helical pipes with a finite pitch. *J. Fluid Mech.*, **251**, 315–353

Liu, S. and Masliyah, J. H. 1993c. Steady developing flows in helical pipes of finite pitch. Submitted

Manlapaz, R. and Churchill, S. W. 1981. Fully developed laminar convection from a helical coil. *Chem. Eng. Commun.*, **9**, 185–200

Murata, S., Miyake, Y., Inaba, T., and Ogawa, H. 1981. Laminar flow in a helically coiled pipe. *Bull. Jpn. Soc. M.E.*, **24**, 355–362

Nandakumar, K. and Masliyah, J. H. 1986. Swirling flow and heat transfer in coiled and twisted pipes. In *Advances in Transport Processes*, Vol. IV, A. S. Mujumdar and R. A. Mashelkar (eds.). Wiley Eastern Ltd., New Delhi

Patankar, S. V., Pratap, V. S., and Spalding, D. B. 1974. Prediction of laminar flow and heat transfer in helically coiled pipes. *J. Fluid Mech.*, **62**, 539–551

Tarbell, J. M. and Samuels, M. R. 1973. Momentum and heat transfer in helical coils. *Chem. Eng. J.*, **5**, 117–127

Tuttle, E. R. 1990. Laminar flow in twisted pipes. *J. Fluid Mech.*, **219**, 545–570

Wang, C. Y. 1981. On the low-Reynolds-number flow in a helical pipe. *J. Fluid Mech.*, **108**, 185–194

Xie, D. G. 1990. Torsion effect on secondary flow in a helical pipe. *Int. J. Heat Fluid Flow*, **11**, 114–119